International Journal of Solids and Structures 50 (2013) 270–278

Contents lists available at SciVerse ScienceDirect

International Journal of Solids and Structures

journal homepage: www.elsevier.com/locate/ijsolstr

Effect of friction on the planar elastica constrained inside a circular channel with clearance

Chih-Wen Liu, Jen-San Chen *

Department of Mechanical Engineering, National Taiwan University, Taipei 10617, Taiwan

ARTICLE INFO

Article history:
Received 4 December 2011
Received in revised form 21 September 2012
Available online 3 October 2012

Keywords:
Friction
Constrained elastica
Circular channel

ABSTRACT

In this paper we consider the effect of friction force on the contact behavior of an elastica inside a circular channel with clearance. The elastica is partially clamped at both the input and output ends of the channel. Coulomb friction is assumed to be present at the output end and on the constraining walls. Focused is placed on the relative motion between the input end and the output end of the elastica. Shooting method is adopted to solve for the quasi-static behavior of the elastica movement. Four types of contact patterns between the elastica and the constraining channel walls may occur when the input end moves in and out of the channel; they are rolling point contact, combined rolling and sliding point contact, rolling line contact, and sliding line contact. When the input end undergoes a sinusoidal motion, the output end either ceases to move at all, or follows exactly the input end motion. These two phases of output end motion occur subsequently, one immediately after the other. In general, the output end lags behind the input end. Experimental observations on the lagging phenomenon at the output end confirm the theoretical prediction.

1. Introduction

The deformation of a planar elastica constrained inside a circular channel with clearance has been investigated by Chen and Li (2007) and Lu and Chen (2008). These previous works were motivated by the need to understand how a guidewire deforms inside human artery housing during stent deployment procedure adopted in treating patients with coronary artery diseases (Schneider, 2003). In these previous papers it was assumed that one end of the guidewire is fixed and the guidewire is allowed to be fed into the circular channel continuously from the other end. This reflects the extreme case when the artery is blocked entirely and the leading end of the guidewire is stuck by the lesion. The friction in the lateral contact between the elastica and the channel wall was neglected in these analyses.

In a less extreme case, and probably a more realistic one, the blockage of the artery is less severe and the leading end of the guidewire is allowed to barely pass through the lesion area. In this case the narrowed passageway exerts a friction force opposing the movement of the guidewire at the leading end. The guidewire deforms and contacts the artery wall while it is continuously fed into or withdrawn from the channel with the input end being controlled by the surgeon's hand movement. The friction between the guidewire and the artery wall also plays a role in the deformation of the guidewire. It is observed in practice that the movement of the leading end of the guidewire near the lesion does not follow exactly the surgeon's hand movement at the input end. This creates a problem for a surgeon in the operating room, and for a control engineer in designing a medical robot. This paper intends to investigate the deformation of the guidewire in this situation. The guidewire is modeled as an elastica, and the artery housing is modeled as a rigid circular channel.

The elastica problem discussed in this paper falls in a field called constrained elastica, which refers to an elastica constrained laterally and forced to deform between a pair of rigid walls. Most of the previous researches in constrained elastica assume that the contact between the elastica and the rigid walls is frictionless (see Feodosyev, 1977; Vaillette and Adams, 1983; Adams and Benson, 1986; Adan et al., 1994; Domokos et al., 1997; Chai, 1998; Holmes et al., 1999; Chen and Li, 2007; Lu and Chen, 2008; Ro et al., 2010).

Effect of friction in constrained elastica was discussed previously by several researchers. Chateau and Nguyen (1991) considered the effect of Coulomb friction and formulated a rate problem leading to some stability criteria. Chai (2002) used a large-strain finite element analysis incorporating a frictional contact algorithm to model the behavior of the constrained elastica. Roman and Pocheau (2002) observed that the contact point shifting was due to either gliding, rolling, or both motions simultaneously. These previous works considered the case when the constraining channel is straight and one end of the elastica is fixed in space.

* Corresponding author. Tel.: +886 2 3366 2693; fax: +886 2 2363 1755.
E-mail address: jschen@ntu.edu.tw (J.-S. Chen).

0020-7683/$ - see front matter © 2012 Elsevier Ltd. All rights reserved.
http://dx.doi.org/10.1016/j.ijsolstr.2012.09.026

In contrast to these previous works, we assume that the elastica is constrained inside a circular channel. Both ends of the elastica are clamped laterally, while the elastica is allowed to pass through the clamps in the longitudinal direction. Focus will be placed on the effect of friction force in the clamp near the leading (output) end, and in the lateral contact between the elastica and the constraining wall on the movement relations between the two ends of the elastica. The knowledge gained in this analysis should prove useful in designing a medical robot for stent deployment in practice.

2. Problem description

Fig. 1 shows a circular channel with outer radius r_o and inner radius r_i. The span angle is ψ. An elastic beam, with flexural rigidity EI, is inserted in the channel with both ends being clamped laterally. In the longitudinal direction, the beam is allowed to pass through the two end clamps A and B. This type of boundary condition may be called "partial" clamp. The elastic beam is inextensible and is stress free when it is straight. It is assumed that the diameter of the elastic beam is negligible compared to the gap $r_o - r_i$ of the channel. The initial deformation of the beam (elastica) is a circular arc with radius of curvature $(r_o + r_i)/2$, as shown by the dashed curve. At the output end B, the clamp exerts a Coulomb friction force against the longitudinal movement of the elastica relative to the clamp. The coefficient of static friction is μ_B. In the special case when $\mu_B = 0$, the elastica will remain circular when the elastica is fed into the channel from end A. The length Δl_B of the elastica exiting from the output end B will be equal to the length Δl_A fed into the input end A. In the case when μ_B is non-zero, on the other hand, the elastica may deform inside the channel and touch the channel walls, as shown by the solid curve. If lateral contact occurs, it is assumed that Coulomb friction with coefficient μ_l develops. Apparently, for this case the lengths Δl_A and Δl_B will not be equal.

3. Contact patterns

3.1. Rolling point contact

We first assume that the friction at end B is large enough that the elastica is stuck at end B first and is forced to deform when the elastica is continuously fed in through end A. The elastica will deform and touch the outer wall at the middle point first. When the elastica continues to be fed in, the contact point will move to the left through rolling first.

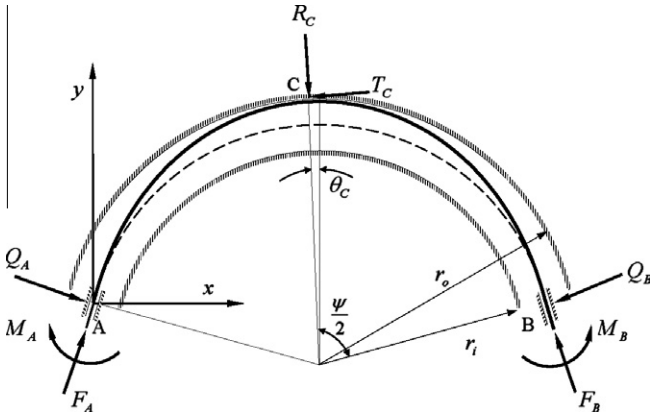

Fig. 1. An elastica in contact with the outer wall at point C. The elastica is assumed to be stuck at point B. Friction is present at point C.

We set an xy-coordinate system with the origin at point A, as shown in Fig. 1. The y-axis points in the bisectional direction of the channel. The contact point C is to the left of the midpoint on the outer wall, with angular position θ_C (positive measured counterclockwise from the y-axis). The elastica is subject to longitudinal force F_A, shear force Q_A, and bending moment M_A at end A. At contact point C, the elastica is under normal force R_C and friction force T_C. We assume that longitudinal force F_A is increased incrementally. At a set F_A, the elastica is in equilibrium. The bending moment $M(s)$ at any point of the elastica can be written as

$$M(s) = EI\frac{d\theta}{ds} = M_A + F_x(s)y - F_y(s)x \tag{1}$$

s is the length of the elastica measured from point A. θ is the rotation angle of the tangent measured from x-axis. $F_x(s)$ and $F_y(s)$ are the internal forces in the x- and y-directions, and can be written as

$$F_x(s) = -F_A\cos\frac{\psi}{2} - Q_A\sin\frac{\psi}{2} + (T_C\cos\theta_C - R_C\sin\theta_c)H(s - s_C) \tag{2}$$

$$F_y(s) = -F_A\sin\frac{\psi}{2} + Q_A\cos\frac{\psi}{2} + (T_C\sin\theta_C + R_C\cos\theta_c)H(s - s_C) \tag{3}$$

H is the Heaviside step function. s_C is the arc length of point C measured from A. For convenience we introduce the following dimensionless parameters (with asterisks):

$$(s^*, x^*, y^*) = \frac{(s, x, y)}{r_o}, \quad (Q_A^*, F_A^*) = \frac{r_o^2}{EI}(Q_A, F_A), \quad M_A^* = \frac{r_o}{EI}M_A \tag{4}$$

Eq. (4) represent the non-dimensionalization schemes for all lengths, forces, and moments in this paper. Similarly, we may introduce the dimensionless distributed force (per unit length) q^*, which will be used later, as

$$q^* = \frac{r_o^3}{EI}q \tag{5}$$

After substituting relations (4) into Eq. (1), and dropping all the superposed asterisks thereafter for simplicity, we obtain the dimensionless equilibrium equation

$$\frac{d\theta}{ds} = M_A + F_x(s)y - F_y(s)x \tag{6}$$

After differentiating Eq. (6) with respect to s and noting the geometric relations

$$\frac{dx}{ds} = \cos\theta \tag{7}$$

$$\frac{dy}{ds} = \sin\theta \tag{8}$$

we obtain

$$\frac{dM}{ds} = F_x(s)\sin\theta - F_y(s)\cos\theta \tag{9}$$

The boundary conditions at point A are

$$x|_{s=0} = 0 \tag{10}$$

$$y|_{s=0} = 0 \tag{11}$$

$$\theta|_{s=0} = \frac{\psi}{2} \tag{12}$$

The boundary conditions at end B are

$$x|_{s=s_B} = (1+\eta)\sin\frac{\psi}{2} \tag{13}$$

$$y|_{s=s_B} = 0 \tag{14}$$

$$\theta|_{s=s_B} = -\frac{\psi}{2} \tag{15}$$

s_B is the arc length of point B measured from A, which can also be interpreted as the length of the elastica inside the channel. At the contact point C, the geometric constraints are

$$x|_{s=s_C} = \frac{(1+\eta)}{2}\sin\frac{\psi}{2} - \sin\theta_C \tag{16}$$

$$y|_{s=s_C} = \cos\theta_C - \frac{(1+\eta)}{2}\cos\frac{\psi}{2} \tag{17}$$

where η is defined as the radius ratio r_i/r_o.

The above differential equations and boundary conditions are not sufficient to solve for all the unknowns when the elastica is in equilibrium. For a nonlinear problem involving Coulomb friction, the equilibrium solutions are dependent upon the loading path. For instance, the friction T_C will be different for loading and unloading processes, even though the elastica may be in the same deformation configuration. For the moment, we assume that the elastica is under loading process. In other words, we consider the situation when the longitudinal force F_A is increased by a small amount ΔF_A.

When the elastica first contacts the middle point of the outer wall, the friction T_C is zero. In the case when the elastica is stuck at end B and continues to be fed in through end A, the elastica must move in some manner. In the first stage, T_C is so small that $\frac{T_C}{R_C} < \mu_l$. Therefore, no sliding occurs at point C. The reasonable assumption is that the elastica rolls on the outer wall when the longitudinal force is increased from $F_A - \Delta F_A$ to F_A.

Fig. 2(a) shows the relation between the elastica and the constraining wall during rolling motion. The dashed and solid curves represent the elastica before and after rolling, respectively. C_1 and C_2 are the contact points on the outer wall. The two black dots represent the same material point, which contacts the outer wall before rolling. Similarly, the two triangles represent the same material point, which contacts the outer wall after rolling. In a rolling motion, the arc length C_1C_2 on the wall, denoted Δs_W, is equal to the length between the two points on the elastica before (dot) and after (triangle) contact, denoted Δs_M. The rolling condition $\Delta s_W = \Delta s_M$ may be written mathematically as

$$s_C = s_{C(b)} + (s_{B(b)} - s_B) - (\theta_{C(b)} - \theta_C) \tag{18}$$

Variables with subscript (b) in Eq. (18) represent the parameters at $F_A - \Delta F_A$.

We use shooting method to solve for the equilibrium solutions. For the problem at hand, we are given μ_l, η, and ψ. We assume that $s_{B(b)}$, $s_{C(b)}$, and $\theta_{C(b)}$ at the force step $F_A - \Delta F_A$ are available. We make a guess on six unknowns: M_A, Q_A, R_C, T_C, s_C, and s_B, and integrate the four Eqs. (6)–(9) for θ, x, y, and M. from $s = 0$ to $s = s_B$. The guessed M_A and Eqs. (10)–(12) are used as initial conditions. Subroutines in Mathematica are used in the integration procedure. The three boundary conditions (13)–(15), and the three rolling contact conditions (16)–(18) are used to check the accuracy of the guesses. If the results are not satisfactory, a new set of guesses is adopted. A Newton–Raphson algorithm is employed to improve the iteration speed. After the solutions are obtained, we check the ratio $\frac{T_C}{R_C}$. If $\frac{T_C}{R_C} < \mu_l$, it means that the rolling motion assumption is valid. On the other hand, if $\frac{T_C}{R_C} > \mu_l$, then rolling contact assumption is not valid, and should be replaced by sliding point condition.

3.2. Sliding point contact

Fig. 2(b) shows the relation between the elastica and the constraining wall during pure sliding motion. Again, the dashed and solid curves represent the elastica before and after sliding motion, respectively. The material point on the elastica in contact with the outer wall remains the same before and after sliding. Therefore, $\Delta s_M = 0$ during pure point sliding. The friction force T_C is acting to oppose this motion as shown. This situation, however, does not happen in the contact problem as described in this paper. Instead, the sliding motion will be combined with rolling, as described in Fig. 2(c) and (d). Fig. 2(c) shows the situation when $\Delta s_W < \Delta s_M$, and Fig. 2(d) shows the case when $\Delta s_W > \Delta s_M$. The friction forces in these two cases are in different directions.

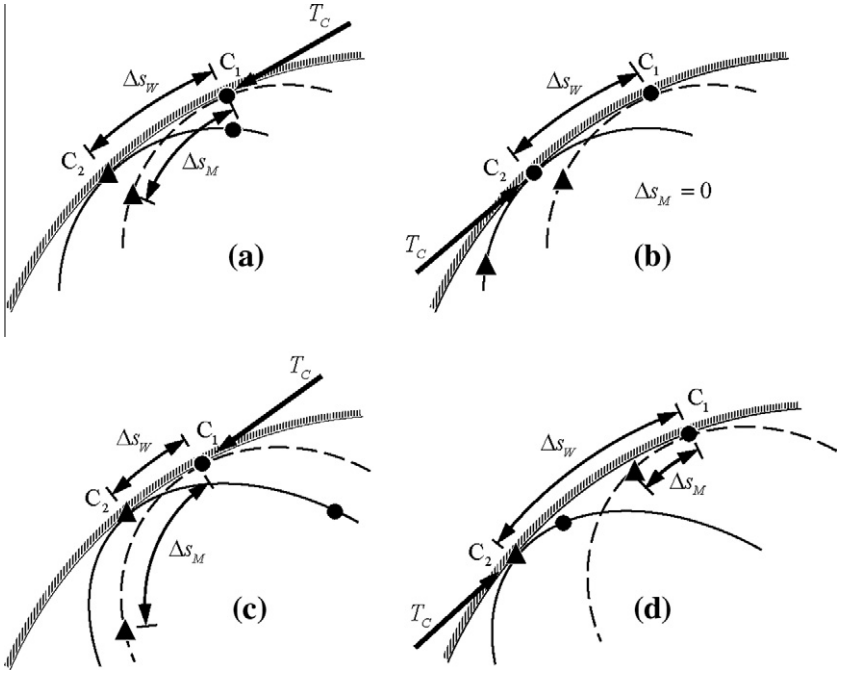

Fig. 2. Point contacts with friction. (a) Pure rolling ($\Delta s_W = \Delta s_M$), (b) pure sliding ($\Delta s_M = 0$), (c) combined rolling and sliding ($\Delta s_W < \Delta s_M$), (d) combined rolling and sliding ($\Delta s_W > \Delta s_M$). C_1 and C_2 are the contact points on the outer wall. The dashed and solid curves represent the elastica before and after motion, respectively.

In the case when contact pattern at point C involves sliding, either in the form of Fig. 2(c) or (d), the friction T_C is known as

$$T_C = \mu_l R_C \tag{19}$$

In the solution method, we make a guess on five unknowns M_A, Q_A, R_C, s_C, and s_B. We integrate the four equations (6)–(9) for θ, x, y, and M from $s = 0$ to $s = s_B$. The guessed M_A and Eqs. (10)–(12) are used as initial conditions. The three boundary conditions (13)–(15), and the two contact conditions (16) and (17) are used to check the accuracy of the guesses.

The point-contact deformation obtained above has to be examined whether the elastica penetrates the constraining wall. In the case when the curvature of the elastica at point C is smaller than the curvature of the outer wall, the point contact deformation should evolve to sliding line contact, as shown in Fig. 3.

3.3. Sliding line contact

In Fig. 3, the elastica contacts the outer wall between points C and D, i.e., from $s = s_C$ to s_D. The angular positions of points C and D are θ_C and θ_D, respectively, measured from the y-axis. In the segments from $s = 0$ to s_C and from s_D to s_B, the elastica is free of contact. At points C and D, the elastica is under concentrated normal force R_C and R_D. Between points C and D, the elastica is under distributed normal force $q(s)$. By the assumption of impending sliding motion, the outer wall exerts concentrated friction forces T_C and T_D at points C and D, respectively, and distributed friction $F_s(s)$. These friction forces are

$$T_C = \mu_l R_C \tag{20}$$

$$T_D = \mu_l R_D \tag{21}$$

$$F_s(s) = \mu_l q(s) \tag{22}$$

In the segment from $s = 0$ to s_C, the internal forces in the x- and y-directions are

$$F_x(s) = -F_A \cos\frac{\psi}{2} - Q_A \sin\frac{\psi}{2} \tag{23}$$

$$F_y(s) = -F_A \sin\frac{\psi}{2} + Q_A \cos\frac{\psi}{2} \tag{24}$$

At the point slightly to the left of point C, one can find the internal forces in the tangential and normal directions as

$$P_{C(L)} = F_A \cos\left(\theta_C - \frac{\psi}{2}\right) - Q_A \sin\left(\theta_C - \frac{\psi}{2}\right) \tag{25}$$

$$Q_{C(L)} = -F_A \sin\left(\theta_C - \frac{\psi}{2}\right) - Q_A \cos\left(\theta_C - \frac{\psi}{2}\right) \tag{26}$$

The subscript (L) in Eqs. (25) and (26) is to emphasize that the forces are to the left of point C. Since the curvature in the line-contact segment is a constant, the bending moment is a constant. Therefore, the shear force in the contact segment is zero. As a consequence, we have

$$R_C = Q_{C(L)} \tag{27}$$

From Eqs. (20) and (27), we conclude that the longitudinal component of the internal force slightly to the right of point C, denoted $P_{C(R)}$, can be written as

$$P_{C(R)} = P_{C(L)} - \mu_l Q_{C(L)} \tag{28}$$

In order to find the distributed contact force in the line-contact segment, we draw a free body diagram of an infinitesimal element between $s = s_C$ and s_D, as shown in Fig. 4. From the force balance in the normal and tangential directions, one can write

$$P\cos\frac{-d\theta}{2} - F_s(-d\theta) - (P + dP)\cos\frac{-d\theta}{2} = 0 \tag{29}$$

$$q(-d\theta) - P\sin\frac{-d\theta}{2} - (P + dP)\sin\frac{-d\theta}{2} = 0 \tag{30}$$

P is the longitudinal compressive force. From Eqs. (22), (29) and (30), after neglecting higher order terms, one can derive

$$dP = \mu_l q d\theta \tag{31}$$

$$P = q \tag{32}$$

Eq. (32) indicates that the transversal contact pressure is only carried by longitudinal force. After substituting Eq. (32) into (31) and integrate from point C, one can derive

$$P(\theta) = P_{C(R)} e^{-\mu_l(\theta_C - \theta)} \tag{33}$$

From Eqs. (32) and (33), we have the expressions of the distributed force in terms of θ,

$$q(\theta) = P_{C(R)} e^{-\mu_l(\theta_C - \theta)} \tag{34}$$

Therefore, the distributed normal force is an exponential function along the line-contact segment of the elastica. It is noted that for a straight channel, the normal contact force is zero within the framework of Euler beam model. Therefore, the distributed force $q(\theta)$ is zero. For a more complicated curved channel, for instance,

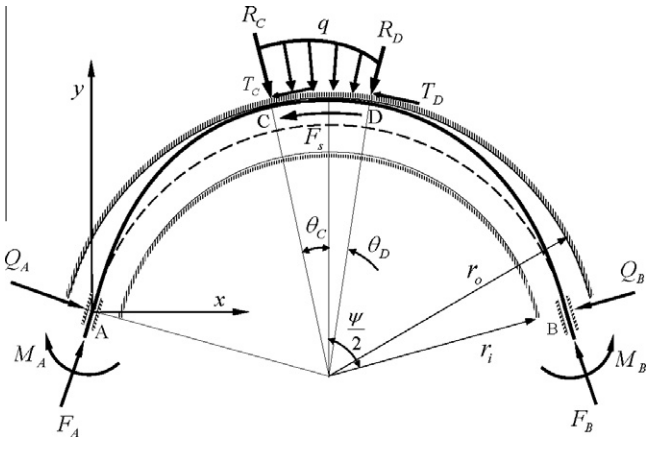

Fig. 3. An elastica in line contact with the outer wall in segment CD. The elastica is assumed to be stuck at point B. The distributed normal force q and the corresponding friction force F_s are not uniform along the line-contact segment.

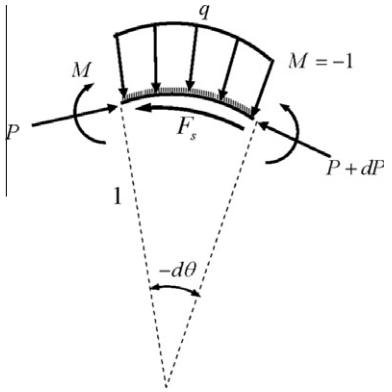

Fig. 4. Free body diagram of a small element of the elastica in sliding line contact with the outer wall.

an elliptic channel, $q(\theta)$ should be in a non-uniform distribution similar to the exponential one, although not exactly the same form as in Eq. (34) mathematically.

The longitudinal force at the point slightly to the left of point D is

$$P_{D(L)} = P_{C(R)} e^{-\mu_l(\theta_C - \theta_D)} \tag{35}$$

From Eqs. (21) and (35) one can obtain the longitudinal force slightly to the right of point D as

$$P_{D(R)} = P_{D(L)} - \mu_l R_D \tag{36}$$

In the segment between $s = s_D$ and s_B, the x- and y-components of the internal force are

$$F_x(s) = -P_{D(R)} \cos\theta_D - R_D \sin\theta_D \tag{37}$$

$$F_y(s) = -P_{D(R)} \sin\theta_D + R_D \cos\theta_D \tag{38}$$

The contact conditions at points C and D are

$$x|_{s=s_\alpha} = \frac{(1+\eta)}{2}\sin\frac{\psi}{2} - \sin\theta_\alpha \tag{39}$$

$$y|_{s=s_\alpha} = \cos\theta_\alpha - \frac{(1+\eta)}{2}\cos\frac{\psi}{2} \tag{40}$$

$$M|_{s=s_\alpha} = -1 \tag{41}$$

$$\theta|_{s=s_\alpha} = \theta_\alpha \tag{42}$$

The subscript α in Eqs. (39)–(42) can be C or D. Since the elastica is inextensible, s_C and s_D are related by

$$s_D = s_C + (\theta_C - \theta_D) \tag{43}$$

In the shooting method, we make a guess on six variables M_A, Q_A, R_D, θ_D, s_C, and s_B. We integrate the four equations (6)–(9) for θ, x, y, and M from $s = 0$ to $s = s_C$ first. Eqs. (23) and (24) are used to calculate the internal forces $F_x(s)$ and $F_y(s)$ in Eqs. (6) and (9). The guessed M_A and Eqs. (10)–(12) are used as initial conditions. Similarly we use Eqs. (39)–(42) (with $\alpha \equiv D$) as initial conditions and integrate equations (6)–(9) from $s = s_D$ to s_B. Eqs. (37) and (38) are used to calculate the internal forces $F_x(s)$ and $F_y(s)$ in the integration from $s = s_D$ to s_B. The three boundary conditions (13)–(15), and the three contact conditions (39)–(41) (with $\alpha \equiv C$) are used to check the accuracy of the guesses.

3.4. Rolling line contact

In some cases, rolling line contact will occur. For instance, rolling line contact will occur when the elastica is unloaded from a sliding line contact. The rolling contact condition at a single point has been spelled out in Eq. (18). When rolling line contact occurs, this condition has to be valid for every point in the line-contact segment because the elastica is inextensible. In particular, the ratio $\mu = F_s/q$ should remain a constant throughout the contact segment, where $|\mu| < \mu_l$.

The solution method for rolling line contact is similar to sliding point contact as discussed in Section 3.3. We make a guess on seven variables M_A, Q_A, R_D, θ_D, s_C, s_B, and μ. We integrate the four Eqs. (6)–(9) from $s = 0$ to $s = s_C$ first. Eqs. (23) and (24) are used to calculate the internal forces $F_x(s)$ and $F_y(s)$ in Eqs. (6) and (9). The guessed M_A and Eqs. (10)–(12) are used as initial conditions. Similarly, we use Eqs. (39)–(42) (with $\alpha \equiv D$) as initial conditions and integrate Eqs. (6)–(9) from $s = s_D$ to s_B. Eqs. (37) and (38) are used to calculate the internal forces $F_x(s)$ and $F_y(s)$ in the integration from $s = s_D$ to s_B. The three boundary conditions (13)–(15), the three contact conditions (39)–(41) (with $\alpha \equiv C$), and Eq. (18) are used to check the accuracy of the guesses.

4. Numerical examples

4.1. Compressive input end force

We consider a circular channel with span angle $\psi = 150°$, radius ratio $\eta = 0.8$. The coefficient of static friction at clamp B is $\mu_B = 1.0$. Fig. 5 shows the relation between the compressive end force F_A at clamp A and the variation Δl of the total length inside the channel,

$$\Delta l = \Delta l_A - \Delta l_B \tag{44}$$

In the solution method, the compressive force increment ΔF_A is set as 0.1. The dashed line and the solid line represent the cases when the coefficient of friction μ_l in lateral contact is set as 0 and 0.5, respectively. It is reasonable to assume that μ_B is greater than μ_l, because μ_B is meant to represent the partial blockage in the lesion area of the blood vessel.

For the case when $\mu_l = 0$, the load–deflection curve starts from the origin and passes through points a, g, and h, all marked with cross marks ×. At point a, the elastica makes a point contact at the middle point of the outer wall. At point g, the point contact evolves to line contact. At point h, the friction force at clamp B exceeds the maximum static friction, and the elastica exits from clamp B. The input force F_A cannot be increased further beyond point h. We define the Δl at point h as the maximum length the input end of the elastica can be inserted in the channel before the output end protrudes out of the channel, denoted $\Delta l^{(C)}_{\max}$. The superscript (C) specifies that this is for the case of compressive input force. For the case when $\mu_l = 0$, $\Delta l^{(C)}_{\max} = 0.165$. If F_A decreases incrementally, the load–deflection curve traces the same path from h, g, a, and back to the origin. No hysteresis occurs in the load-unload cycle.

For the case when $\mu_l = 0.5$, the load–deflection curve starts from the origin and passes through points b, c, d, marked by black dots. From the origin to point a, no contact occurs. From a to b the elastica is in rolling point contact with the outer wall. This segment is very small, and is magnified in the inset. At point b, the rolling point contact evolves to sliding point contact until point c. At point c, the sliding point contact evolves to sliding line contact. At point d, the friction force at clamp B exceeds the maximum static friction, and F_A cannot be increased further. For this case $\Delta l^{(C)}_{\max}$ is the length increment at point d, which is 0.174.

If the pushing force F_A decreases incrementally, the load–deflection curve traces points d, e, f, a, and back to the origin. From point d to e, the elastica is in rolling line contact. At point e the contact pattern evolves to rolling point contact. At point f, the rolling point contact evolves to sliding point contact until point a. Apparently, hysteresis occurs within a load-unload cycle.

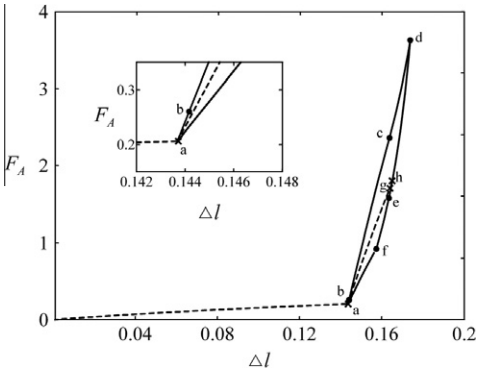

Fig. 5. Relation between the input compressive force F_A and the elastica length variation inside the channel Δl. Coefficient of friction μ_B at the output end is 1.0. The dashed and solid lines represent the cases when μ_l, the friction coefficient on the lateral wall, are 0 and 0.5, respectively.

4.2. Tensile input end force

In Fig. 5 the input force F_A is compressive. In the surgery, the surgeon may need to extract the guidewire away from the artery. Fig. 6 shows the relation between tensile F_A and the total length variation Δl. Again, the dashed and solid curves represent the cases when the coefficient of friction μ_l in the lateral contact is set as 0 and 0.5, respectively.

For the case when $\mu_l = 0$, the load–deflection curve starts from the origin (outside the range of Fig. 6) and passes through points i, n, and o. At point i, the elastica contacts the middle point on the inner wall. At point n, the point contact evolves to line contact on the inner wall. At point o, the friction force at clamp B exceeds the maximum static friction. At this point the elastica retracts from clamp B, and the tensile force F_A cannot be increased further. The Δl at point o is defined as the maximum length the input end of the elastica can be extracted from the channel before the output end is pulled inside the channel, denoted $\Delta l^{(T)}_{\max}$. The superscript (T) specifies that this is for the case of tensile input force. For the case when $\mu_l = 0$, $\Delta l^{(T)}_{\max} = 0.164$.

For the case when $\mu_l = 0.5$, the load–deflection curve starts from the origin and passes through points i, j, and k. After making a point contact at point i, the elastica experiences a rolling motion first. The rolling motion evolves to sliding point contact immediately after point i. The range of rolling point contact is so small that it cannot be shown in Fig. 6. The sliding point contact evolves to sliding line contact at point j. At point k, the friction force at clamp B exceeds the maximum static friction, and the tensile force F_A cannot be increased further. For this case $\Delta l^{(T)}_{\max}$ is the length variation at point k, which is 0.168. It is interesting to note that $\Delta l^{(C)}_{\max}$ is slightly different from $\Delta l^{(T)}_{\max}$ even for the same μ_l.

If the tensile force F_A decreases incrementally, the load–deflection curve traces points k, l, m, i, and back to the origin. From point k to l, the elastica is in rolling line contact with the inner wall. At point l the contact pattern evolves to sliding line contact. At point m, the sliding line contact evolves to sliding point contact until point i.

Several conclusions regarding the effects of the constraining wall friction can be summarized by comparing the dashed and solid curves in Figs. 5 and 6. First of all, larger F_A is needed to push or pull the elastica in order for the elastica to exit or retract from clamp B when the friction on the constraining wall is present. This is natural because the constraining wall friction force is to hinder the relative motion between the wall and the elastica. Secondly, when the input force F_A is under a load-unload cycle, the load–deflection curves exhibits hysteresis behavior. Therefore, for a specified Δl_A at the input end, the deformation of the elastica depends on whether the corresponding input force F_A is increasing or decreasing. Thirdly, the motion of the elastica at the output end is lagging behind the input end when friction at clamp B is present. This poses difficulty for the surgeon in placing the leading (output) end of the guidewire accurately through controlling the input end motion at point A.

4.3. Sinusoidal input end motion

The solid curve in Fig. 7(a) represents the input end motion history Δl_A of the elastica at end A. We assume that the input end is undergoing two cycles of sinusoidal motion with amplitude 0.3. Points R_1, R_2, R_3, and R_4 represent the reversing points of the solid curve. Starting from the origin O_1, the elastica is being pushed in the channel through end A until point R_1, and then being retreated and pulled out of the channel until point R_2, etc. The dashed curve represents the corresponding output end motion (Δl_B) at B. μ_B and μ_l are set as 1.0 and 0.5, respectively. The dots on the solid and dashed curves correspond to the points on the solid curve of Figs. 5 and 6. Only significant points on the curves are shown. Obviously, the motion of end B is lagging behind.

At the origin O_1, the elastica is in its original circular shape with $F_A = 0$. Starting from O_1, the elastica contacts the outer wall first at point a. Through rolling and sliding motions, the elastica overcomes all the friction forces and extrudes out from end B at point

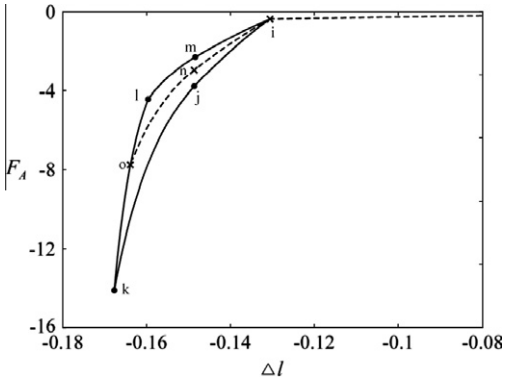

Fig. 6. Relation between the input tensile force F_A and the elastica length variation inside the channel Δl. Coefficient of friction μ_B at the output end is 1.0. The dashed and solid lines represent the cases when μ_l, the friction coefficient on the lateral wall, are 0 and 0.5, respectively.

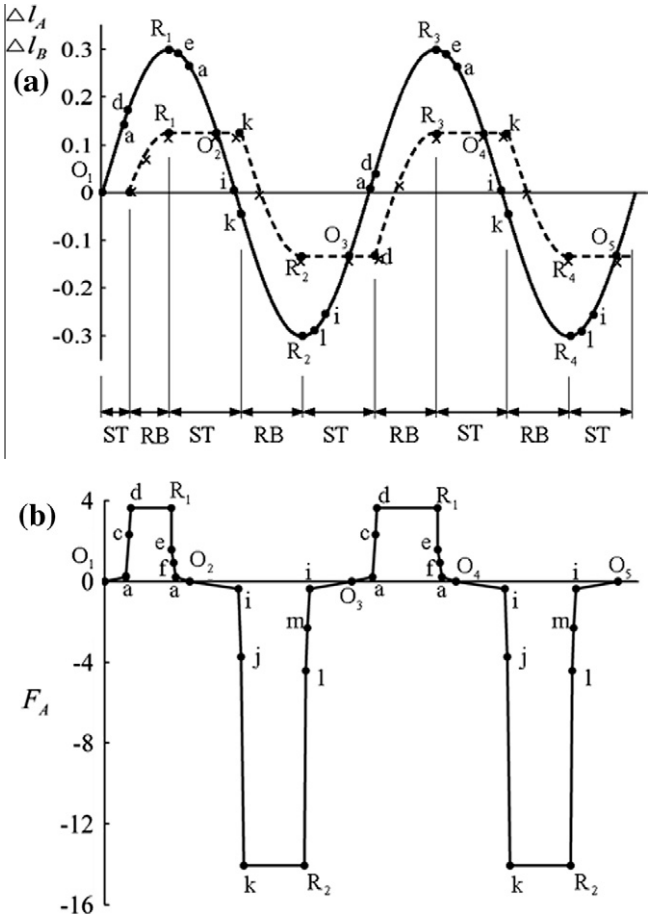

Fig. 7. (a) Input end motion (solid, Δl_A) and output end motion (dashed, Δl_B) when the input end is under a sinusoidal motion. ST means that the eastica is stuck at end B. RB means that the elastica moves like a rigid body. The cross marks represent experimental results. (b) The corresponding input end longitudinal force F_A.

d. Starting from point d until point R_1, the elastica is in sliding line contact with the outer wall. In this interval, the elastica moves like a rigid body and the output end follows exactly the motion of the input end. The elastica is then extracted from the input end starting from the first reversing point R_1, and passing points e and a. Starting from point a, the elastica ceases to contact the channel wall. At point O_2, the elastica returns to the original circular shape with $F_A = 0$. The corresponding F_A history is shown in Fig. 7(b).

Starting from point O_2, the elastica continues to be drawn out of the channel from end A until it makes a point contact with the inner wall at point i. It is noted that Δl_A at i is not zero, although it is very small. Through rolling and sliding subsequently, the elastica overcomes all the friction forces and retracts from end B at point k. Starting from point k until point R_2, the elastica is in sliding line contact with the inner wall. In this interval, the elastica moves like a rigid body. Starting from point R_2 to point i, the elastica makes rolling and sliding contacts with the inner wall when it is pushed in. From point i to O_3, the elastica ceases to contact the channel. At point O_3, the elastica returns to its original circular shape.

Several conclusions may be summarized from Fig. 7. First of all, in the case when the input end motion is sinusoidal, the output end is periodic, although not in the sinusoidal form. Secondly, the amplitude of the output end motion is smaller than the input end. In Fig. 7 the amplitude of the output end motion is 0.126 on the top and 0.132 in the valley, considerably smaller than 0.3 of the input end motion. Thirdly, the output end motion either ceases to move at all or follows exactly the motion of the input end. These two phases of output end motion occurs subsequently, one immediately after the other. In Fig. 7, the output end does not move from O_1 to d. It then follows exactly the motion of the input end from d to R_1. From R_1 to k, the output end ceases to move. From k to R_2, the output end follows exactly the input end motion again. In the range when the output end follows exactly the input end, the elastica moves like a rigid body. In the range when the output end is stuck, the elastica deforms continuously inside the channel when the input end continues to move in or move out. In Fig. 7(a), ST means that the eastica is stuck at end B, and RB means that the elastica moves like a rigid body.

The relative motion between the input and output ends as described in Fig. 7 is rather typical. However, certain parameter changes may affect the behavior slightly. First of all, the amplitude of the input end motion will affect the behavior of the output end motion of the elastica. For instance, in the case when the amplitude of the input end is reduced to below 0.16, then the output end will not move at all. Secondly, the coefficient of static friction μ_B at clamp B will affect the contact patterns on the lateral walls. For instance, if μ_B is reduced to 0.5, the same as μ_l, then there will not be any line contact on the walls. The lagging phenomenon of the output end relative to the input end remains, although the amplitude of the output end variation decreases slightly.

5. Experimental observations

In order to verify the theoretical prediction, we construct an experimental set-up to observe the lagging phenomenon in the output end, as shown in Fig. 8. The channel is made of two blocks of acrylic glass milled into circular shapes. The inner and outer radii of the acrylic glass channel are 8 and 10 cm, respectively. The span angle $\psi = 150°$. The elastica is made of carbon steel (type SK5) with Young's modulus 205 GPa. The cross section of the elastica is 46 mm × 0.1 mm. The friction coefficient μ_l between the acrylic glass and the metallic strip is estimated to be 0.5 by an inclined-plane experiment. At the output end (on the right), we use two aluminum blocks with paper lining to simulate the clamping condition. The gap between the two aluminum blocks can be adjusted by a micro-stage to ensure that the elastica passes through the clamp smoothly. The friction coefficient μ_B between the metallic strip and the paper lining is in the order of 1.0. The clamping device at the input end (on the left) is similar, although less critical. In the experiment, the metallic strip is fed into or retracted from the channel through the input end slowly by hand. The amplitude of the input end movement is 3 cm. The extruding and retracting movements of the metallic strip at the input and output ends are measured by rulers. The results are recorded in Fig. 7 with cross marks. It is found that the observed lagging phenomenon at the output end agrees with the theoretical prediction reasonably well.

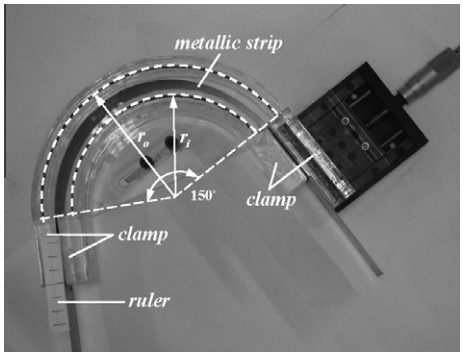

Fig. 8. Experimental set-up.

6. Parameter study

In Sections 4 and 5, the discussion is limited to a specific example in which the span angle $\psi = 150°$, radius ratio of the gap $\eta = 0.8$, friction coefficients on the lateral wall $\mu_l = 0$ and 0.5, and $\mu_B = 1$. In this section, more numerical simulations are conducted for a wider range of these geometric and friction parameters. This parameter study provides more insights into the behavior of the constrained elastica subject to friction.

Fig. 9 shows the relation between the friction coefficient μ_B at end B and the maximum length $\Delta l^{(C)}_{\max}$ of the elastica which can be inserted inside the channel before the output end exits the channel for various span angles ψ. μ_l is set at 0.5 and $\eta = 0.8$. For a point between symbols ● and ■, the elastica is in point contact with the outer wall when protrusion occurs. For a point beyond

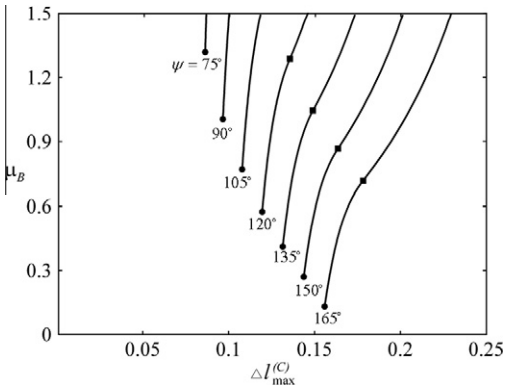

Fig. 9. Relation between μ_B and $\Delta l^{(C)}_{\max}$ for various span angles ψ. μ_l is set at 0.5 and $\eta = 0.8$. For a point between symbols ● and ■, the elastica is in point contact with the outer wall when protrusion occurs. For a point beyond symbol ■, the elastica is in line contact with the outer wall when protrusion occurs.

symbol ■, the elastica is in line contact with the outer wall when protrusion occurs. For a specific span angle ψ, if the friction coefficient μ_B is too small (for instance $\psi = 120°$ and $\mu_B = 0.3$), then the elastica will remain circular shape and exit the channel for any amount of input from the left end. It is said that $\Delta l^{(C)}_{max}$ does not exist in this case. In another example when $\psi = 165°$ and $\mu_B = 0.3$, $\Delta l^{(C)}_{max} = 0.159$. This means that the elastica will exit the channel after the elastica is fed in $\Delta l_A = 0.159$ from the left end. When the protrusion occurs, the elastica is in point contact with the outer wall. Apparently, $\Delta l^{(C)}_{max}$ increases as the span angle increases. The behavior of $\Delta l^{(T)}_{max}$ when the elastica is pulled out of the channel is similar.

One interesting fact observed from the above numerical simulation is that the maximum excess length $\Delta l^{(C)}_{max}$ needed to feed the system before the rod exits the channel is zero if friction coefficient μ_B is under a threshold. Once μ_B is greater than this threshold, $\Delta l^{(C)}_{max}$ has a finite value. This fact is due to the particular behavior of Coulomb friction. When μ_B is smaller than the threshold, the friction resistance at end B is insufficient to maintain static equilibrium of the elastica. Therefore, the rod exits channel for any amount of input from the left end. The elastica remains circular and $\Delta l^{(C)}_{max}$ is zero in this case. In the case when μ_B is greater than the threshold, end B is able to provide sufficient friction resistance to maintain further elastic deformation superposed on the original circular shape of the rod. Once the friction resistance is overcome when the input force is large enough, the elastica starts to slide. Since in Coulomb friction model the maximum static friction resistance is a constant and independent of the input force once sliding occurs, the deformation of the rod slides like a rigid body and $\Delta l^{(C)}_{max}$ has a certain finite value. In general, this finite $\Delta l^{(C)}_{max}$ is larger when μ_B is greater.

Fig. 10 shows the relation between μ_B and $\Delta l^{(C)}_{max}$ for various gap ratios η. In this figure μ_l is set at 0.5 and $\psi = 150°$. It is noted that the μ_B of all the black dots are the same. In other words, the μ_B at which protrusion of the elastica starts to occur is independent of the gap ratio η. Apparently, for a wider gap (smaller η), $\Delta l^{(C)}_{max}$ is larger. This is expected because wider gap provides more room for the rod to undergo bending deformation, which reduces the longitudinal force transferred from the input end to the output end. In general, $\Delta l^{(C)}_{max}$ is between $\psi(1-\eta)/4$ and $\psi(1-\eta)/2$. In the limit case when η is close to 1, this range is very small, and the curve in Fig. 10 is close to a vertical straight line.

Fig. 11 shows the relation between μ_B and $\Delta l^{(C)}_{max}$ for various μ_l. In this figure η is set at 0.8 and $\psi = 150°$. This figure indicates that for larger μ_l, the $\Delta l^{(C)}_{max}$ is larger. It is noted that all curves in this figure originated from the same black dot ●. This means that the μ_B at which protrusion of the elastica starts to occur is independent of μ_l, in addition to η as observed in Fig. 10. Furthermore, the $\Delta l^{(C)}_{max}$ is independent of μ_l as well.

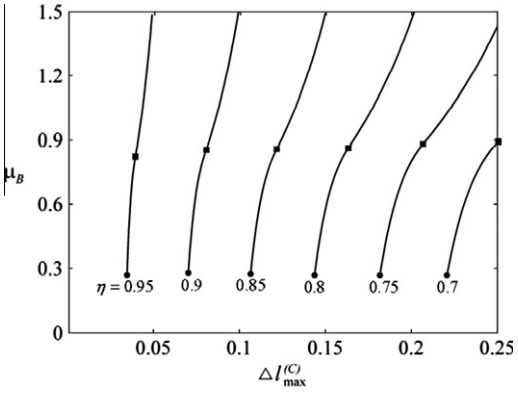

Fig. 10. Relation between μ_B and $\Delta l^{(C)}_{max}$ for various gap ratios η. μ_l is set at 0.5 and $\psi = 150°$. For a point between symbols ● and ■, the elastica is in point contact with the outer wall when protrusion occurs. For a point beyond symbol ■, the elastica is in line contact with the outer wall when protrusion occurs.

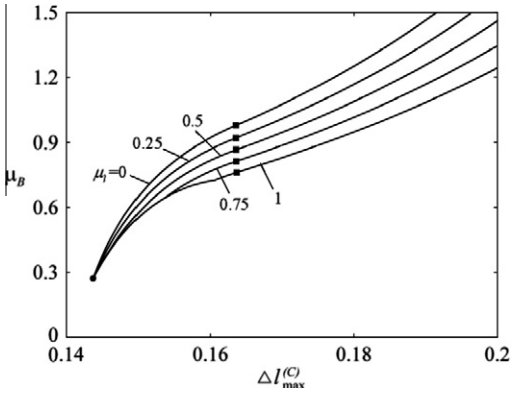

Fig. 11. Relation between μ_B and $\Delta l^{(C)}_{max}$ for various friction coefficient on the wall μ_l. η is set at 0.8 and $\psi = 150°$. For a point between symbols ● and ■, the elastica is in point contact with the outer wall when protrusion occurs. For a point beyond symbol ■, the elastica is in line contact with the outer wall when protrusion occurs.

One interesting fact observed from the above numerical simulation is that the maximum excess length needed to feed the system before the rod exits the channel $\Delta l^{(C)}_{max}$ is zero if friction coefficient μ_B is under a critical value.

7. Conclusions and discussions

In this paper we consider the effect of friction force on the contact behavior of an elastica inside a circular channel with clearance. The elastica is meant to represent a guidewire in the stent deployment procedure, and the circular channel is meant to represent part of a blood vessel. The elastica is partially clamped at the input end and the output end of the channel. Coulomb friction is assumed to be present on the lateral walls of the channel and at the output end, which represents partial blockage in the lesion area of the blood vessel. Focus is placed on the relative motion between the input end, which is controlled by surgeon's hand movement, and the output end. Shooting method is adopted to solve for the quasi-static behavior of the elastica motion. Experiments are conducted to verify the theory. The effects of friction may be summarized as follows:

(1) Four types of contact patterns between the elastica and the constraining channel walls may occur when the input end moves in and out of the channel; they are rolling point contact, combined rolling and sliding point contact, rolling line contact, and sliding line contact. In the case when friction on the lateral wall is present, the deformation is asymmetric.
(2) When line contact with friction occurs, the distributed force exerted by the constraining wall onto the elastica is not uniform. Instead, the force distribution is an exponential function along the elastica.
(3) Hysteresis occurs when the input end undergoes a load-unload cycle. In other words, the load–deflection curve forms a closed loop in a load-unload cycle.
(4) When the input end is undergoing a sinusoidal motion, the output end will exhibit periodic motion, although not sinusoidal any more. The output end either ceases to move at all, or follows exactly the input end motion. These two phases of output end motion occur subsequently, one

immediately after the other. In general, the output end lags behind the input end. Experimental observations on the lagging phenomenon at the output end confirm the theoretical prediction.

It is noted that in this paper we neglect the thickness of the guidewire. In the case when the thickness of the wire is not negligible, the contact behavior is more complicated. However, it is reasonable to estimate $\Delta l^{(C)}_{\max}$ by taking into account the smaller effect gap due to the thickness of the wire.

In the extreme case when μ_B is very large, the right end is effectively fully clamped. The behavior of the constrained elastica in this extreme case when μ_l is zero was studied in a previous paper by Chen and Li (2007). This paper is therefore an extension of that paper for the case when the clamp friction is less extreme. The elastica inside circular channel deforms continuously, without buckling, under the action of end longitudinal force. This is significantly different from the case of straight channel, in which repeated buckling will occur (Domokos et al., 1997). This is because the two end forces are aligned perfectly in the straight case, which allows the straight configuration (a trivial solution) to exist. In the circular case, no matter how small the curvature is, the end longitudinal forces are not aligned and trivial solution does not exist.

References

Adams, G.G., Benson, R.C., 1986. Postbuckling of an elastic plate in a rigid channel. Int. J. Mech. Sci. 28, 153–162.
Adan, N., Sheinman, I., Altus, E., 1994. Post-buckling behavior of beams under contact constraints. ASME J. Appl. Mech. 61, 764–772.
Chai, H., 1998. The post-buckling behavior of a bilaterally constrained column. J. Mech. Phys. Solids 46, 1155–1181.
Chai, H., 2002. On the post-buckling behavior of bilaterally constrained plates. Int. J. Solids Struct. 39, 2911–2926.
Chateau, X., Nguyen, Q.S., 1991. Buckling of elastic structures in unilateral contact with or without friction. Eur. J. Mech. A 1, 71–89.
Chen, J.-S., Li, C.-W., 2007. Planar elastica inside a curved tube with clearance. Int. J. Solids Struct. 44, 6173–6186.
Domokos, G., Holmes, P., Royce, B., 1997. Constrained Euler buckling. J. Nonlinear Sci. 7, 281–314.
Feodosyev, V.I., 1977. Selected Problems and Questions in Strength of Materials. Mir, Moscow (Translated from the Russian by M. Konyaeva).
Holmes, P., Domokos, G., Schmitt, J., Szeberenyi, I., 1999. Constrained Euler buckling: an interplay of computation and analysis. Comput. Method Appl. M 170, 175–207.
Lu, Z.-H., Chen, J.-S., 2008. Deformations of a clamped–clamped elastica inside a circular channel with clearance. Int. J. Solids Struct. 45, 2470–2492.
Ro, W.-C., Chen, J.-S., Hung, S.-Y., 2010. Vibration and stability of a constrained elastica with variable length. Int. J. Solids Struct. 47, 2143–2154.
Roman, B., Pocheau, A., 2002. Postbuckling of bilaterally constrained rectangular thin plates. J. Mech. Phys. Solids 50, 2379–2401.
Schneider, P.A., 2003. Endovascular Skills: Guidewire and Catheter Skills for Endovascular Surgery. Marcel Dekker, Inc., New York.
Vaillette, D.P., Adams, G.G., 1983. An elastic beam contained in a frictionless channel. ASME J. Appl. Mech. 50, 693–694.